Engineering Geology 100 (2008) 43–58

Contents lists available at ScienceDirect

Engineering Geology

journal homepage: www.elsevier.com/locate/enggeo

Statistical approach to earthquake-induced landslide susceptibility

Chyi-Tyi Lee [a,*], Chien-Cheng Huang [b], Jiin-Fa Lee [b], Kuo-Liang Pan [a], Ming-Lang Lin [c], Jia-Jyun Dong [a]

[a] Institute of Applied Geology, National Central University, No.300, Jungda Road, Jungli City, Taoyuan County, 32001, Taiwan
[b] Central Geological Survey, Ministry of Economic Affairs, No.2, Lane 109, Huashin Street, Chungho City, Taipei County, 23500, Taiwan
[c] Department of Civil Engineering, National Taiwan University, No.1, Sec. 4 Roosevelt Road, Taipei, 10617, Taiwan

ARTICLE INFO

Article history:
Received 19 November 2007
Received in revised form 27 February 2008
Accepted 4 March 2008
Available online 18 March 2008

Keywords:
Landslides
Landslide inventory
Event-based
Landslide susceptibility
Landslide hazard
Chi-Chi earthquake
Earthquake-induced landslides

ABSTRACT

Susceptibility analysis for predicting earthquake-induced landslides has most frequently been done using deterministic methods; multivariate statistical methods have not previously been applied. In this study, however, we introduce a statistical methodology that uses the intensity of earthquake shaking as a landslide triggering factor. This methodology is applied in a study of shallow earthquake-induced landslides in central western Taiwan. The results show that we can accurately interpret landslide distribution in the study area and predict the occurrence of landslides in neighboring regions. This susceptibility model is capable of predicting shallow landslides induced during an earthquake scenario with similar range of ground shaking, without requiring the use of geotechnical, groundwater or failure depth data.

1. Introduction

The study of earthquake-induced landslide susceptibility on a regional scale commonly requires the employment of an analytical slope-stability method and the infinite-slope model (Wilson and Keefer, 1985; Jibson and Keefer, 1993; Harp and Wilson, 1995; Jibson et al., 1998, 2000; Liao, 2004). This method requires calculation to determine the limit-equilibrium of the slope stability given the strength parameters, failure depth, and groundwater conditions for every calculation point in the study area. This requirement causes immense problems in terms of data acquisition and control of spatial variability of the variables (Hutchinson, 1995; Guzzetti et al., 1999).

In traditional landslide susceptibility analysis (LSA), it is most common to use a statistical approach where landslide inventories and causative factors are utilized to build a susceptibility model for the prediction of future landslides. Many different methods and techniques for assessing landslide hazards have been proposed and tested. These have already been systematically compared and their advantages and limitations outlined (Carrara, 1983; Varnes, 1984; Carrara et al., 1995; Hutchinson, 1995; Chung and Fabbri, 1999; Guzzetti et al., 1999; Chung, 2006; van Western et al., 2006; Keefer and Larsen, 2007). Most of these approaches require multi-temporal landslide inventories so that the susceptibility model can predict landslide occurrence over a given time period (Guzzetti et al., 1999).

In the study of earthquake-induced landslides, the landslide inventory is naturally event-based; it is not possible to use a multi-temporal landslide inventory. Therefore, the temporal significance of a susceptibility model should incorporate the use of a triggering factor, like that used in the deterministic method. In this study, we demonstrate our new method using an example. We first look at data from the Kuohsing area in central western Taiwan, where many landslides were triggered by the 1999 Chi-Chi earthquake (Liao and Lee, 2000). The results are then validated by looking at an example from the neighboring Tungshih area.

2. Regional setting

The island of Taiwan has an area of 36,000 km^2. The highest peak is Yushan, which is 3952 m above sea level, and there are numerous other peaks over 3000 m. Taiwan is tectonically active being on the collision zone between the Asiatic continent and the Luzon Arc (Chai, 1972; Bowin et al., 1978; Teng, 1990). Active crustal deformation (Bonilla, 1975, 1977; Yu et al., 1997), frequent earthquakes (Hsu, 1971; Tsai et al., 1977; Wu, 1978), numerous typhoons and a high erosion rate (Dadson et al., 2003) presently characterize the rapid earth altering processes and changing landforms of the region.

* Corresponding author.
E-mail addresses: ct@ncu.edu.tw (C.-T. Lee), huangcc@linx.moeacgs.gov.tw (C.-C. Huang), leejfa@linx.moeacgs.gov.tw (J.-F. Lee), klpan168@ms38.hinet.net (K.-L. Pan), mlin@ntu.edu.tw (M.-L. Lin), jjdong@geo.ncu.edu.tw (J.-J. Dong).

0013-7952/$ – see front matter © 2008 Elsevier B.V. All rights reserved.
doi:10.1016/j.enggeo.2008.03.004

The study area, comprised of the Kuohsing and Tungshih quadrangles, is located in central western Taiwan, falling partly in the Western Foothills Geologic Province (western part) and partly in the Hsueshan Range Sub-province of the Central Range Geologic Province (eastern part) (Fig. 1). Kuohsing is east of the Taichung Basin, where metropolitan Taichung is located, and west of the Central Range. Tungshih is located immediately north of Kuohsing. The Kuohsing quadrangle and the Tungshih quadrangle are fitting to the national 1/50,000 scale map sheet, and are 705.3 km^2 and 703.9 km^2 in area, respectively.

Geologically, the Western Foothills are characterized by fold-and-thrust Neogene sedimentary strata; the Hsueshan Range is typically

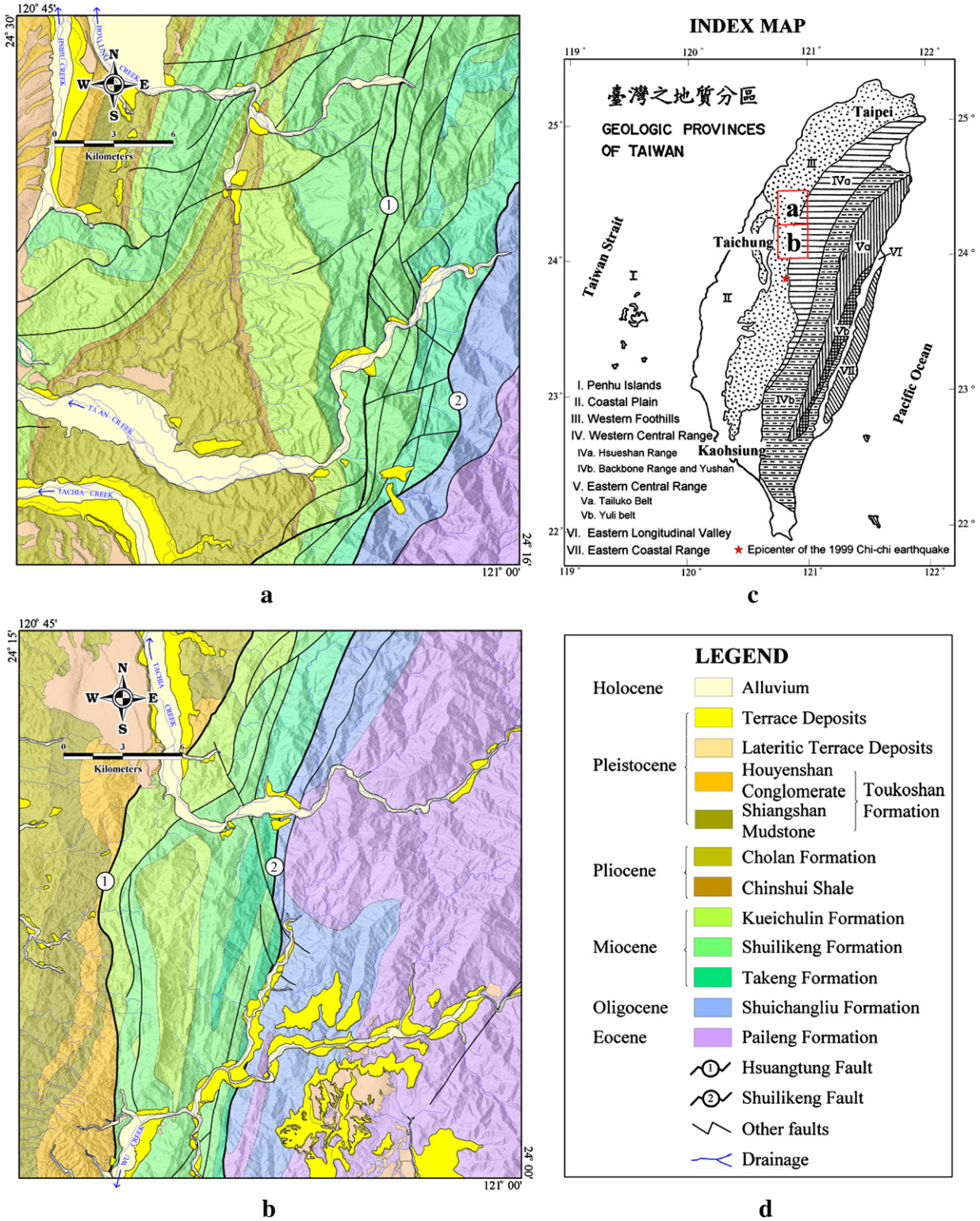

Fig. 1. Location and geology of the study sites: (a) geologic map of Tungshih quadrangle; (b) geologic map of Kuohsing quadrangle; (c) geologic provinces of Taiwan and index map; (d) legend for geologic maps.

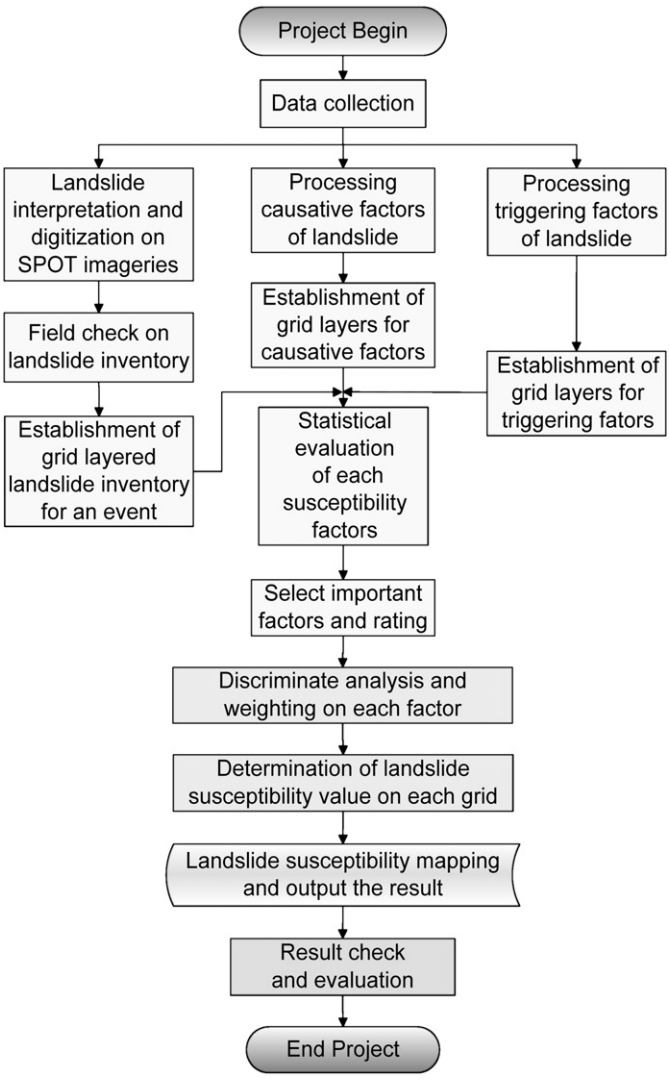

Fig. 2. Working procedure for event-based landslide susceptibility analysis.

characterized by a Paleogene slate belt of argillite and quartzitic sandstone (Ho, 1975). The Shuilikeng Fault forms a boundary between these two provinces. Geomorphically, the study area can be divided into two types of terrains, a western hilly terrain and an eastern mountainous terrain, divided by the Hsuangtung Fault (Fig. 1). The altitudes in the hilly terrain are generally less than 500 m, and the rocks consist of weakly-cemented Pliocene and Pleistocene mudstone, sandstone and conglomerate. The elevation in the mountainous terrain is generally greater than 500 m with many peaks exceeding 1000 m, while the rocks consist of better-indurated Eocene, Oligocene and Miocene, sandstone, shale, argillite and quartzite. The geomorphic appearance in the hilly terrain is more fragmented with shorter slope length, while the mountainous terrain is more solid with longer length of slopes. Typical slope gradients in the hilly terrain are between 10° and 30°, with a mode of about 16°, while in the mountainous terrain, typical slope gradients are between 10° and 45°, with a mode of about 26°.

The climate in the study area is subtropical with an average annual precipitation of about 2400 mm, and an average of 159 rainy days per year. Approximately three typhoons strike this area each year, mostly between July and October. The heaviest rainfall typically occurs in June, July and August; with a monthly average during that period of about 400 mm. The dry season is from October through March with a monthly precipitation average of about 80 mm, and a monthly average of about 8 rainy days. Landslides are common in the study area, especially during an earthquake or typhoon event. They became an even bigger problem after the 1999 Chi-Chi earthquake, during subsequent typhoons. Debris flows and sediment transport became a major problem that governmental authorities had coped with.

The epicenter of the September 21,1999 Chi-Chi earthquake (moment magnitude M_w 7.6) was located about 15 km south of the study area (Ma et al., 1999; Kao and Chen, 2000) (Fig. 1c). Surface fault-rupture occurred along the Chelungpu fault about 3 km west of the Kuohsing quadrangle and extended into the southwest corner of the Tungshih quadrangle. All of the Kuohsing quadrangle and most of the Tungshih quadrangle are located on the hanging wall of the Chelungpu fault, where thrust movement occurred. These areas suffered from severe shaking during the main shock and aftershocks of the Chi-Chi earthquake sequence.

9272 large landslides of various types (with areas greater than 625m^2), with a total area of 127.8 km^2 were triggered by the Chi-Chi earthquake (Liao and Lee, 2000). Of these, 1316 landslides, with a total area of 22.03 km^2, were triggered in the Kuohsing quadrangle, and 1623 landslides, with a total area of 11.97 km^2, were triggered in the Tungshih quadrangle.

3. Methodology

This study is one element of an investigation of landslides in Taiwan by the Central Geological Survey (CGS) of Taiwan (Lee et al., 2005). The aim of the overall CGS investigation is to produce a set of landslide susceptibility maps (scale: 1/25,000) for Taiwan. Since this is a target-oriented project, the methodology for producing the landslide susceptibility maps must be objective and simple, and meet the needs of future work. These criteria are satisfied by the use of discriminant analysis of multivariate statistics, as well as an event-based landslide inventory derived from high resolution satellite images taken before and soon after the triggering event.

The working procedure for LSA is illustrated in Fig. 2. The first step is data collection, after which an event-based landslide inventory is established. In parallel with this, the causative factors of the landslides are processed and the triggering factors determined. These factors are then statistically tested, and the most effective are selected for susceptibility analysis. Each selected factor is rated, and their weighting analyzed. Discriminant analysis allows us to determine the maximum difference for each factor between the landslide group and the non-landslide group, as well as the apparent weights of the factors. After this, a landslide susceptibility index (LSI) for each grid point is calculated from the linear weighted summation of all factors. The LSIs are then used for landslide susceptibility mapping. Because the landslide inventory used is event-based, this LSA is called event-based LSA (EB-LSA).

This procedure must be performed separately for each type of terrain, because of differences in their geomorphic and geologic characteristics. In our case, hilly terrain and mountainous terrain have to be considered separately.

Table 1
SPOT images used in the Chi-Chi earthquake event

Site	Event date	Image	Time	Series number	Type
Kuohsing	1999/09/21	Before	1999/04/01	G0012701	XS
			1999/04/01	G0013125	PAN
		After	1999/09/27	G0013087	XS
			1999/09/27	G0013091	PAN
Tungshih	1999/09/21	Before	1999/04/01	G0012463	XS
			1999/04/01	G0014023	PAN
		After	1999/10/31	I1991031	XS
			1999/10/31	M1991031	PAN

3.1. Data acquisition

The basic data utilized in this study included a 40 m × 40 m grid digital elevation model (DEM), SPOT images, 1/5000 photo-based contour maps, 1/50,000 geologic maps, and earthquake strong-motion records.

The DEMs used were collected by the Aerial Survey Office of Taiwan's Forestry Bureau. They were visually checked by comparing them with a color-shaded image. When a defect of more than a few pixels in size was found, this portion was re-digitized from a 1/5000 scale photo-based contour map. Other abnormal random points were corrected using a median filter. Finally the DEMs were interpolated to a grid of 20 m × 20 m cells using cubic spline interpolation. Raster cells 20 m × 20 m in size were used for all later processing and analysis for each landslide instability factor.

Selected SPOT images taken before and after the Chi-Chi earthquake event are shown on Table 1. All SPOT images were received,

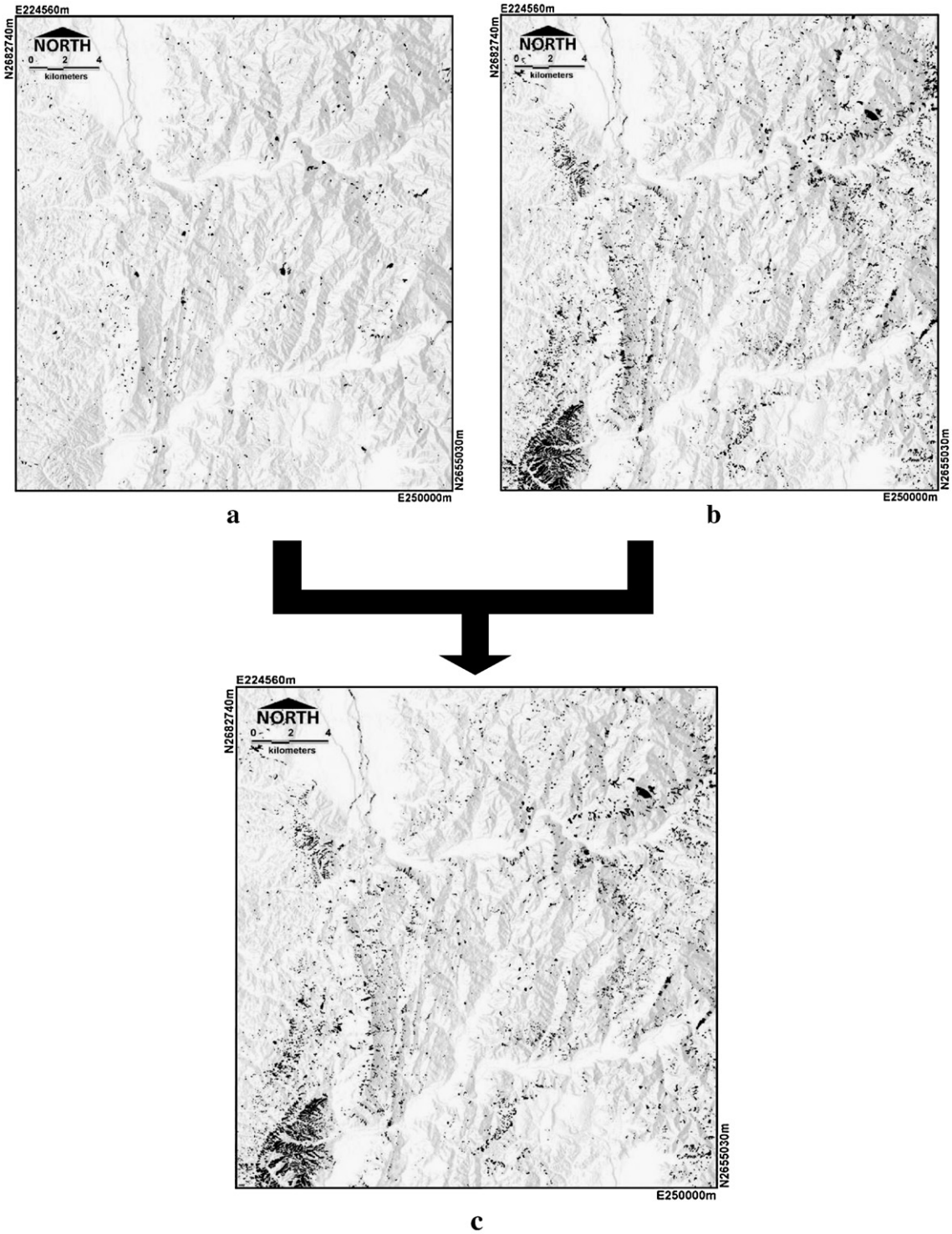

Fig. 3. Extraction of landslides triggered by an event, example from the Kuohsing quadrangle: (a) landslides before the Chi-Chi earthquake; (b) landslides after the Chi-Chi earthquake; (c) landslides triggered by the Chi-Chi earthquake.

processed and rectified by the Center for Space and Remote Sensing Research, National Central University. Both multi-spectral (XS) and panchromatic (PAN) images were used. A fusing technique (Liu, 2000) was utilized to produce a higher resolution false-color composite image to facilitate landslide recognition. The pixel resolution after fusing was 6.25m.

1/50,000 geological maps were collected from the CGS. Each map was overlaid with a shaded DEM and visually inspected in a Geographic Information System (GIS). Some abnormal boundaries, mostly associated with alluvial and terrace deposits, were corrected. The ERDAS IMAGINE system (ERDAS, 1997) was used to transform the geologic vector map to a raster image.

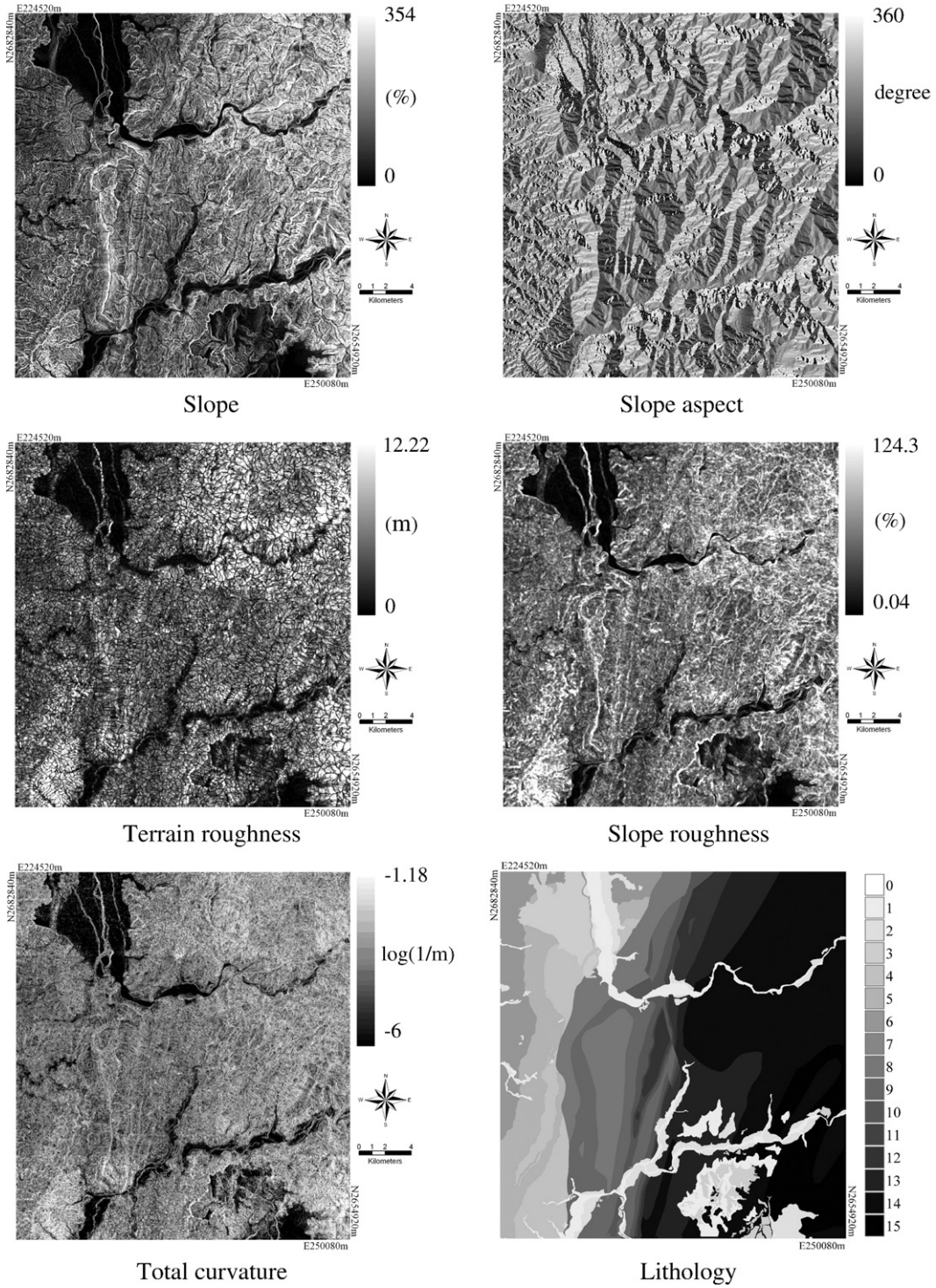

Fig. 4. Spatial distribution of original values of causative factors in the Kuohsing quadrangle. Lithologic unit: 1. Alluvium; 2. Terrace Deposits; 3. Lateritic Terrace Deposits; 4. Toukoshan Formation (conglomerate dominate); 5. Toukoshan Formation (sandstone and shale dominate); 6. Cholan Formation; 7. Kueichulin Formation; 8. Fulungyuan Formation; 9. Hourdonqkeng Formation; 10. Shihmentsum Formation; 11. Takeng Formation, Tanliaoti Member; 12. Takeng Formation, Shihszeku Member; 13. Shuichangliu formation; 14. Paileng Formation, Meitzulin Member; 15. Paileng Formation, Tungmou Member. The formation names in 8–10 are local names for the Shuilikeng Formation as shown in Fig. 1.

Strong-motion seismograms in and around the study area were collected by the Central Weather Bureau, Taiwan. Base-line correction and filtering of the data were performed according to the standard procedure suggested by the Pacific Earthquake Engineering Research Center (PEER) (Darragh et al., 2004). The Arias intensity (Arias, 1970) was then calculated from each corrected seismogram. The arithmetical mean of the Arias intensities of the N–S and E–W components were used to represent the earthquake intensity for the strong-motion station site. These values were interpolated on each grid point in the study area using the ordinary Kriging method (Goovaerts, 1997).

3.2. Event-based landslide inventory

Fused false-color SPOT images taken before and just after the Chi-Chi earthquake (Table 1) were used for landslide recognition. Image interpretation was based on image tone, shape, association, and also personal experience (Pan et al., 2004). At the same time, the landslides were digitized in GIS, and attributes assigned to establish a landslide map table. Each landslide table was then checked against recent rectified aerial photographs via the GIS. Most misinterpretations due to man-made features or cultivated land could be recognized during this comparison. The landslide tables were further modified using ground truth obtained by a field check. A complete pre-event landslide inventory and post-event landslide inventory was formed. Landslide types were noted after examining the characteristics of the landslide's shape, scarring, and deposition on SPOT images, photo-based maps, and by field checking. These data were also recorded as attributes for each landslide object in the GIS. The size of the landslides ranged from about 0.1 to 10 ha with a maximum of 28 ha and a minimum of 0.01 ha. The landslide inventory shows an inverse relationship between the logarithmic number of landslides and landslide size, and shows sound record above 0.4 ha. Neither rock avalanches nor slump type landslides were found within the study area. Most of the landslides were of the shallow translational slide type, some were of the fall type at scarp slopes. The largest landslide in size located at north eastern corner of the Kuohsing quadrangle; it was also field checked to be shallow colluvium slide; bedrocks have exposed on the slope after the slide.

Finally, after a comparison of the pre-event landslide inventory and the post-event inventory, event-triggered landslides identified, and an event-based landslide inventory produced. An event-induced landslide could be absent from the pre-event landslide inventory, or present in both inventories. Landslides found in both inventories were

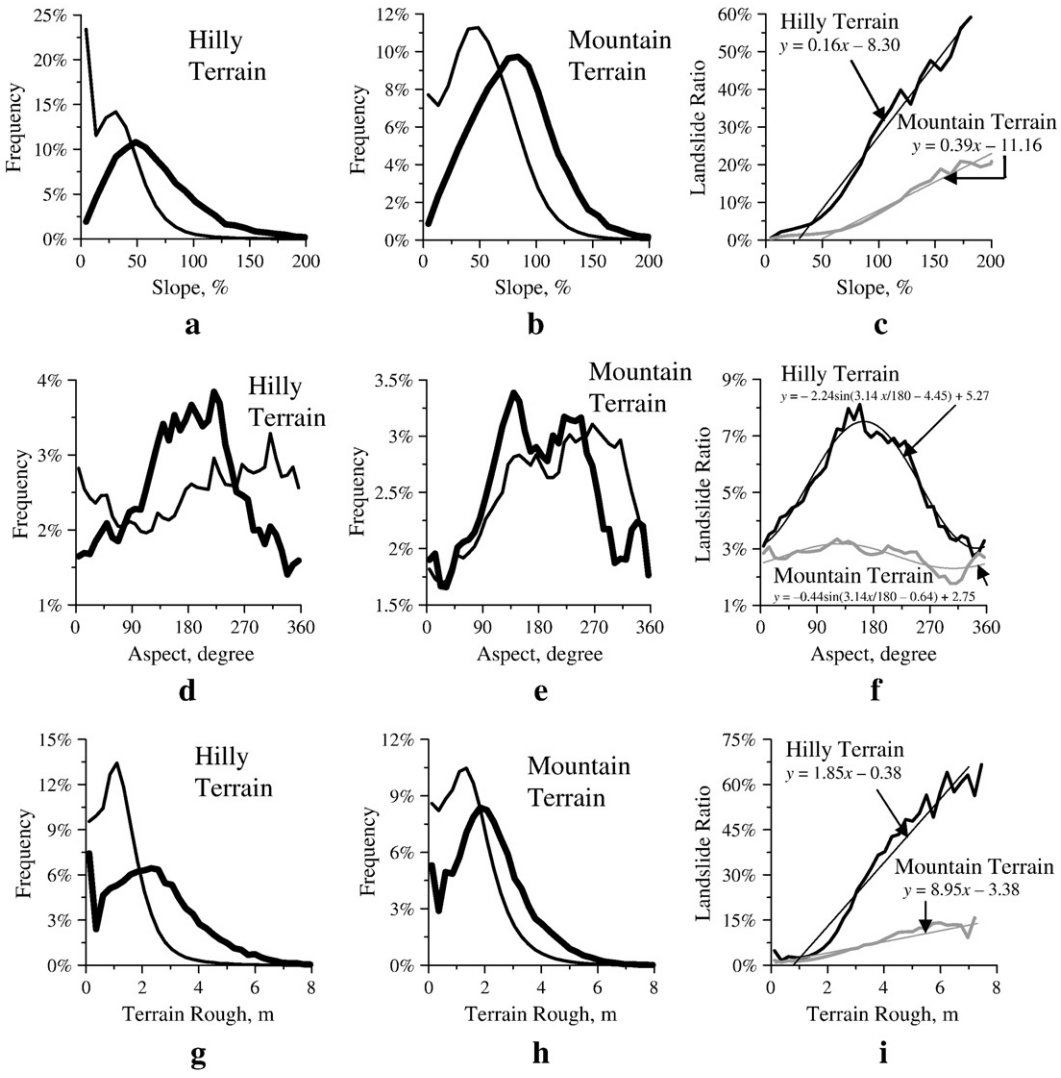

Fig. 5. Frequency distribution of the landslide and non-landslide groups and the landslide ratio of different factors for the Chi-Chi earthquake event for different terrains in the Kuohsing quadrangle: left column (a, d, g, j, m, p) for hilly terrain; middle column (b, e, h, k, n, q) for mountainous terrain. Thick line indicates the landslide group, and thin line indicates the non-landslide group. Right column (c, f, i, l, o, r) shows landslide ratio for both terrains, regression lines are indicated. The landslide ratio is defined as the number of landslide pixels to total pixel in an interval for a factor. Numbering for lithologic units in p, q, r are described in Fig. 4.

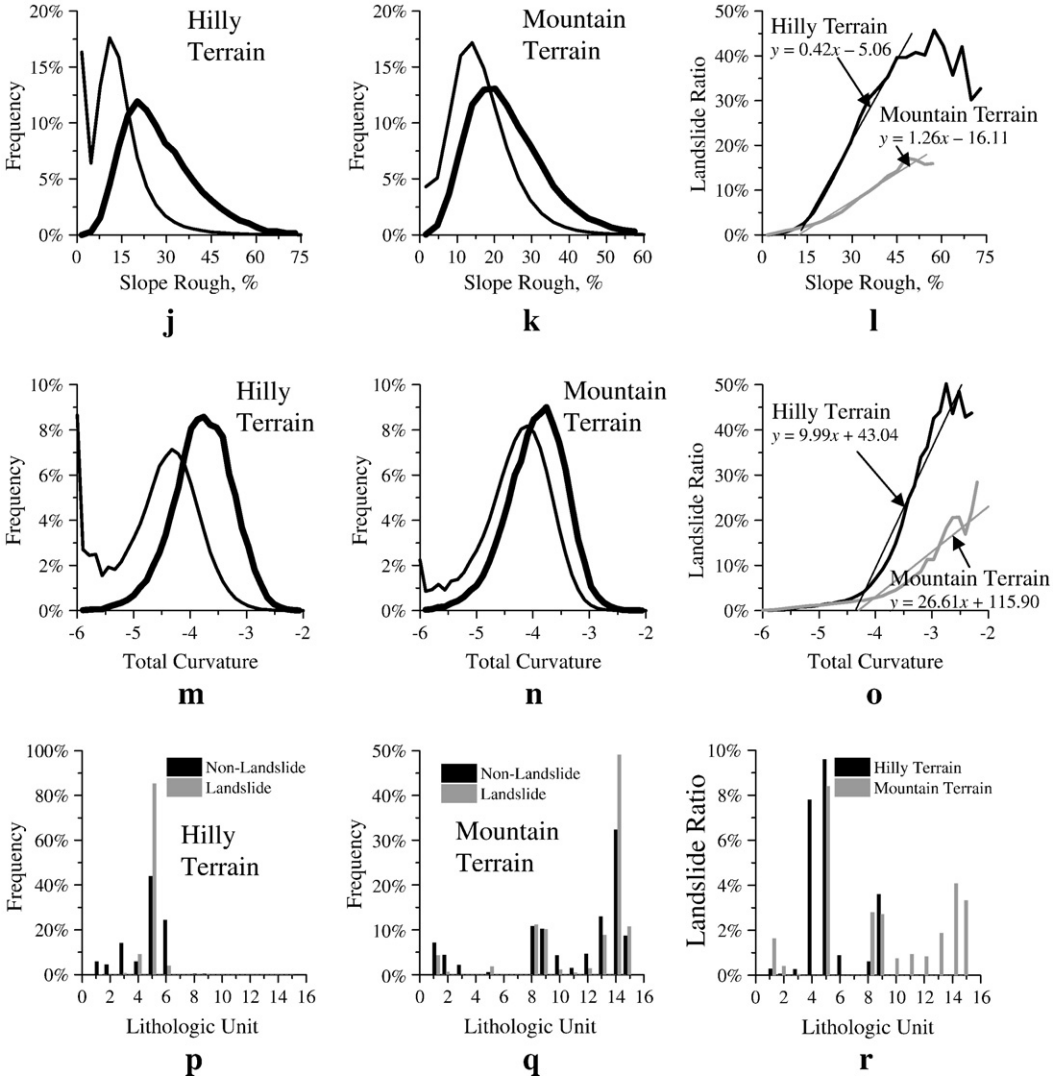

Fig. 5 (*continued*).

examined very carefully for changes in tone and/or enlargement of extent (Pan et al., 2004). The Chi-Chi earthquake event-based landslide inventory for the Kuohsing quadrangle is shown in Fig. 3.

We found that landslide deposit areas should be included in the landslide mapping procedure. Since potential landslide sources are of interest in susceptibility analysis, only source areas may be used to train the susceptibility model. Therefore, we had to differentiate between source areas and actual deposit areas, by assigning them different map objects and attributes. Landslide deposits were identified by comparing the GIS landslide layer with the 1/5000 scale photo-based contour map. The slope angle or concentration of contour lines was used to differentiate deposits from sources.

The final GIS inventory included a detailed description of the date/event, and the size and the type of each landslide object. Only shallow landslides (including rock falls), which included all of the landslides in the study area, were used in the susceptibility analysis. Deep seated slides and rock avalanches (located outside the present study area) and debris flows were studied in a separate project.

3.3. Processing and rating of landslide causative factors

There are more than fifty different landslide-related factors commonly used (both in Taiwan and worldwide) for LSA (Lin, 2003). We selected fourteen of the most frequently used, based on abundance and accessibility. The causative factors were the lithology, slope gradient, slope aspect, terrain roughness, slope roughness, total curvature (Wilson and Gallant, 2000), local slope height, total slope height, topographic index (Kirkby, 1975), distance from a road, distance from a fault, distance from a river head, distance from a river bend, and the normalized differential vegetation index (NDVI, Paruelo et al., 2004).

All these factors were processed by a raster GIS — ERDAS IMAGINE system. The data set was divided into landslide group and the non-landslide group for each terrain. Data for each group and each factor was then classed into intervals and the number of data in each interval recorded to plot the frequency distribution of the data. These results were visually inspected and statistically tested. The effectiveness of the factors as discriminators can be determined by computing the standardized differences for each factor (Davis, 2002)

$$D_j = \frac{\overline{A}_j - \overline{B}_j}{S_{Pj}}, \tag{1}$$

where $\bar{A}_j$ is the mean of factor j for group A (landslide); $\bar{B}_j$ is the mean of factor j for group B (non-landslide); S_{Pj} is the pooled standard

Table 2
Parameters of the main shock and 6 major aftershocks of the Chi-Chi earthquake

Original time (GMT)		Magnitude (M_W)	Epicenter location		Depth (km)
Date	Time		Latitude	Longitude	
1999/9/20	17:47:15	7.30	23.853°	120.816°	8.0
1999/9/20	18:03:40	6.57	23.792°	120.876°	3.5
1999/9/20	18:11:52	6.70	23.850°	121.060°	1.0
1999/9/20	18:16:16	6.66	23.844°	120.039°	1.1
1999/9/20	21:46:37	6.59	23.602°	120.821°	0.3
1999/9/22	00:14:40	6.80	23.826°	121.047°	15.6

deviation of factor j; and D_j is standardized difference of factor j. The larger the standardized difference, the more effective the factor is for differentiating between landslide and non-landslide groups. An effective factor may also be positively correlated with the proportion of landslide cells (Jibson et al., 2000) or the landslide ratio (landslide pixels to total pixels ratio in a factor interval) (Lee et al., 2005). On this basis, of the fourteen causative factors, six (lithology, slope gradient, slope aspect, terrain roughness, slope roughness, and total curvature) were finally selected for the EB-LSA of the earthquake-induced landslides.

Both the slope gradient and the slope aspect were calculated based on the common definitions in the ERDAS IMAGINE system. Terrain roughness at a given point was defined as the standard deviation of elevations within a certain distance (Wilson and Gallant, 2000); in this case, a radius of 3pixels. The data were high-pass filtered before calculation of the terrain roughness. Slope roughness was defined as the standard deviation of slope gradients within a certain radius. We also used a radius of 3pixels for this factor. The definition of total curvature was the same as that used by Wilson and Gallant (2000).

The spatial distribution of the values of the six causative factors is shown in Fig. 4. The frequency distributions for each factor for the landslide group and the non-landslide group, as well as the landslide ratio for each selected factor are shown in Fig. 5. We can see a positive

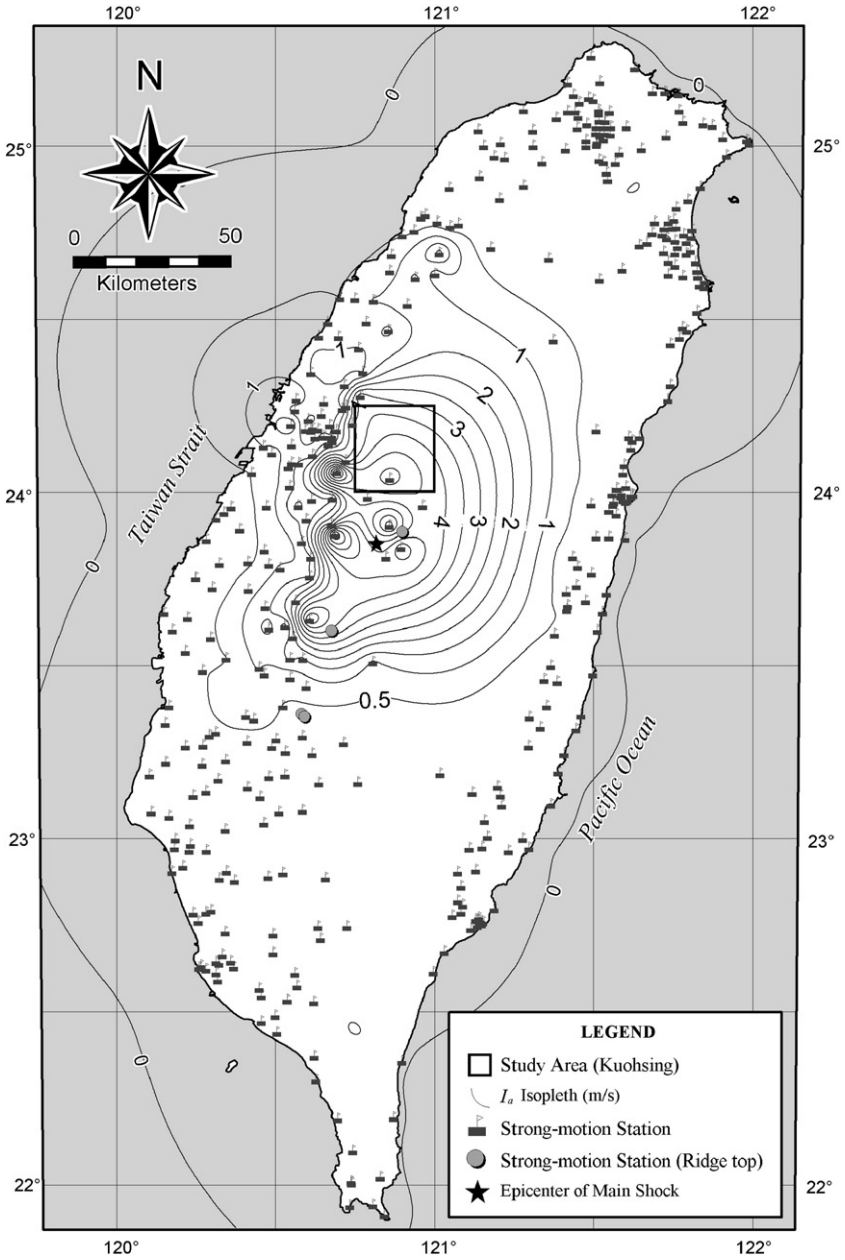

Fig. 6. Arias intensity isopleth of the main shock of the Chi-Chi earthquake. Strong-motion stations with indication of ridge top stations, earthquake epicenter, and the study area are shown.

correlation between landslide ratios and all factors, for both hilly and mountainous terrain (Fig. 5c, f, i, l, o, r). For example (Fig. 5a–c), there exists a threshold value for a gentle slope and an upper limit for a steep slope; a straight line may be fitted only between the threshold value and the upper limit (see Fig. 5c).

Each factor was rated according to its landslide ratios; higher landslide ratio corresponding to a higher rating. We assign a score of 0 if the slope gradient is less than or equal to the lower bound, and a score of 1 if the slope gradient is greater than or equal to the upper bound; the rest are assigned a score between 0 and 1 according to the curve fit. Other factors are determined in a similar manner. There is also a lower and upper bound to the landslide ratio curve. It is necessary to determine these bounds, then fit a curve between them, before a final rating is given. Although the lithology factor data are categorical in nature, a landslide ratio can also be found for each lithologic unit, and a normalized score between 0 and 1 assigned.

3.4. Processing and rating of landslide triggering factors

The triggering factors associated with earthquake shaking are related to intensity. These may include peak ground acceleration (PGA), peak ground velocity (PGV), and Arias intensity (AI), all of which can be obtained from the earthquake strong-motion record. Previous work has shown that landslide probability is proportional to the Newmark displacement (Jibson et al., 2000). Since the Newmark displacement is proportional to the AI (Jibson, 1993; Jibson et al., 1998), the landslide probability should also be proportional. Here we adopted AI as the triggering factor. AI is given by

$$I_a = \frac{\pi}{2g}\int_0^{T_d} (a(t))^2 dt, \tag{2}$$

where g is the acceleration due to gravity; $a(t)$ is the recorded acceleration time-history; and T_d is the duration of the ground motion (Arias, 1970). Dimensionally, AI is a velocity.

The AI for each station was determined by correcting and processing the strong-motion records of the main shock of the Chi-Chi earthquake and 6 major aftershocks. Since the landslide inventory of the Chi-Chi event was made from the SPOT images taken 6days after the main shock, the 6 major aftershocks (Table 2) that occurred within this time also needed to be taken into consideration. Interpolation by the ordinary Kriging method was performed on the data, at each grid point, for each earthquake. Fig. 6 shows the distribution of AI for the Chi-Chi main shock; stations located on the tops of ridges (as indicated in the figure) were not included in the interpolation.

Each grid point was checked to find the maximum AI among the 7 earthquakes, and these values were adopted as the intensity that triggered the landslides. Fig. 7a shows these maximum values. In fact, all the maximum values came from the main shock. Fig. 7b and c shows the distribution of the landslide and non-landslide groups, and the landslide ratio with respect to AI.

We further considered topographic effects in relation to earthquake intensity. The height relative to riverbed (height of the grid point above the riverbed) was found to be a good factor for making corrections, following the empirical formula proposed by Lin and Lee (2003)

$$I_a' = f I_a, \tag{3}$$

$$f = \sqrt{h/93.8 + 0.287} + 0.464, \tag{4}$$

where I_a is the AI; I_a' is the corrected AI; f is the amplification factor; and h is the height relative to riverbed in meters. Data on height above the riverbed are shown in Fig. 7d. Fig. 7e and f show the frequency distributions and the landslide ratio for comparison. The Arias intensity after topographic correction can be seen in Fig. 7g. The frequency distribution of the landslide group and non-landslide group as well as the landslide ratio for the corrected Arias intensity is shown in Fig. 7h and i. It becomes clear that correcting the Arias intensity substantially improves the correlation between the landslide ratio and the AI parameter.

Similar to the method described above for causative factors, we assign an Arias intensity rating with bounds determined according to the landslide ratio. In this case, it is necessary to assign a slightly higher upper bound than the data itself. It is useful for predicting landslides triggered by large intensity earthquake.

3.5. Discriminant analysis

When applying the multivariate method in EB-LSA, we must first find the best linear equation, which gives the greatest separation between the two groups (i.e. landslide group and non-landslide group), with the least inflation on each group (Davis, 2002). The best linear equation (the discriminant function equation) has the form

$$\lambda_i = \sum_j w_j F_{ij}, \tag{5}$$

where $\lambda_i$is the discriminant score at the ith point; w_j is the coefficient of the linear discriminant function for the jth factor; and F_{ij} is the value or the rating of the jth factor at the ith point. All the terms (factors) are added together to yield a single number — the discriminant score.

During analysis, the data set are first divided into group A (landslide) and group B (non-landslide), respectively. We then calculate the pooled variance and covariance matrix **S**, and the difference between the two multivariate means, to form a vector **D**, which can be described as

$$\mathbf{D} = \bar{\mathbf{A}} - \bar{\mathbf{B}}, \tag{6}$$

where $\bar{\mathbf{A}}$ is the multivariate mean for group A; $\bar{\mathbf{B}}$ is the multivariate mean for group B; and

$$\mathbf{S} = \frac{\mathbf{S}_A + \mathbf{S}_B}{n_a + n_b - 2}, \tag{7}$$

where $\mathbf{S}_A$ is the variance and covariance matrix of group A; $\mathbf{S}_B$ is the variance and covariance matrix of group B; n_a is the number of data points in group A; and n_b is the number of data points in group B. Solving the following equation:

$$\mathbf{SW} = \mathbf{D}, \tag{8}$$

allows us to determine the coefficient vector **W**,

$$\mathbf{W} = <w_1, w_2, w_3, \ldots, w_j>. \tag{9}$$

If all the factors in LSA are independent, we may utilize the coefficients as weights. In this case, we need to consider unbiasedness, so that the total weight is equal to unity, i.e.,

$$\sum_j w_j = 1. \tag{10}$$

Because all the factors have already been normalized to be between 0 and 1, the discriminant score λ should also range from 0 to 1 (evaluate Eq. (5)). We further take λ as a susceptibility index for hazard evaluation. These susceptibility indices can now be used to find the landslide spatial probability and mapping.

4. Results and evaluation

An event-based landslide inventory was carried for the Kuohsing quadrangle. The two terrain zones, hilly terrain and mountainous

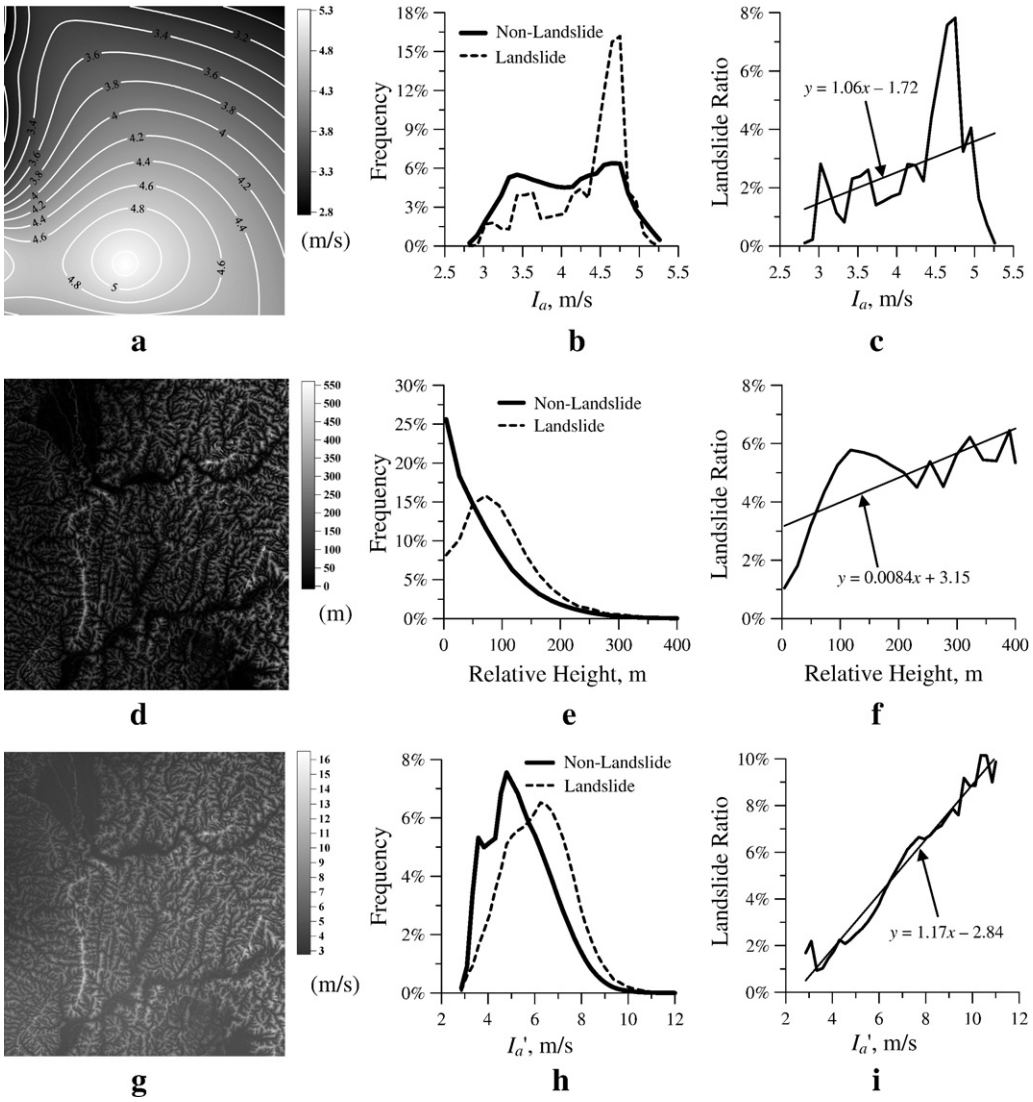

Fig. 7. Spatial distribution of the Arias intensity and frequency distribution of the landslide and non-landslide groups and the landslide ratio for the Chi-Chi earthquake event in the Kuohsing quadrangle. (a) Original Arias intensity; (b) distribution of landslide and non-landslide groups with original Arias intensity; (c) landslide ratio vs. original Arias intensity; (d) height of slope relative to riverbed; (e) distribution of landslide and non-landslide groups with relative height above riverbed; (f) landslide ratio vs. height relative to riverbed; (g) corrected Arias intensity; (h) distribution of landslide and non-landslide groups with corrected Arias intensity; (i) landslide ratio vs. corrected Arias intensity.

terrain, were analyzed separately. The landslide group and a randomly selected non-landslide data set of similar size were used in the discriminant analysis. The results of this analysis include the coefficients of discriminant functions (Table 3). The coefficient of a discriminant function indicates the apparent weighting of each factor, which contributes to the landslide susceptibility at a given point. Of the 7 factors used, it was found that slope gradient, terrain roughness, and the Arias intensity, were weighted the largest for both terrains, but lithology had also a large weight in hilly terrain.

These coefficients were used with Eq. (5) to calculate the LSI for each grid point, which in turn are used to calculate the landslide ratio for each LSI class. The spatial probability of landslide occurrence is indicated by the relation between the landslide ratio (probability of failure) and the LSI (Fig. 8). The relation generally follows a Weibull distribution. The fitting curve is also shown in Fig. 8. There are some fluctuations in the landslide ratio when the susceptibility value is higher, simply because there is less data available. The spatial probability of a landslide is then used to map the susceptibility classes, as shown in Fig. 9.

Gentle slopes (where the slope gradient is less than 10%) can be regarded as stable. In this study, gentle slopes greater than 1 ha in area was regarded as stable, so, were neither used in the discriminant analysis nor in the evaluation of the success rate or prediction rate of the results.

4.1. Success rate for the Kuohsing quadrangle

If we compare actual landslides that occurred during the Chi-Chi earthquake with those on the susceptibility map (Fig. 9), we observe a general agreement between the landslide pattern and areas of high susceptibility. We then used the prediction rate curve method (Chung and Fabbri, 2003) to examine how well the classification results fit the data.

Table 3
Coefficients of the discriminant function for each terrain in the Kuohsing quadrangle

Terrain	Litho	Slope	Slope Asp	Terra Rou	Slope Rou	Total curve	Arias Inten
Hilly	0.141	0.149	0.037	0.146	0.014	0.095	0.419
Mountain	0.082	0.403	0.025	0.136	0.051	0.061	0.242

Note: Litho: lithology. Slope: slope gradient. Slope Asp: slope aspect. Terra Rou: terrain roughness. Slope Rou: slope roughness. Total Curve: total curvature. Arias Inten: Arias intensity. See text for detailed descriptions.

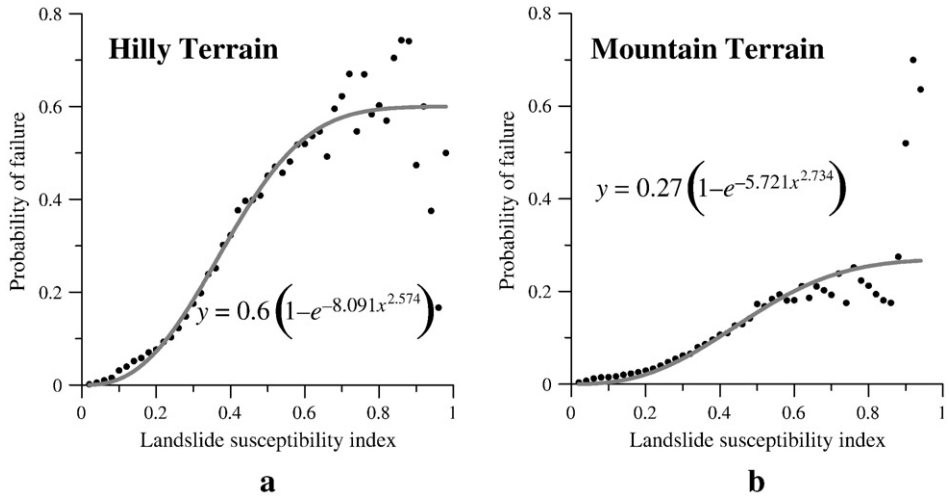

Fig. 8. Distribution of landslide ratio (probability of failure) with respect to landslide susceptibility index in the Kuohsing quadrangle. Weibull distribution curves are shown: (a) hilly terrain; (b) mountainous terrain.

Landslide data used to establish the model were grouped to several classes according to their LSI first, the number of landslide pixels in each class was then divided by total number of pixels in that class, and a cumulative curve was plotted. The prediction rate curve method used in this way is computing a success rate curve (Chung and Fabbri, 1999). The success rate curves for the two terrains are

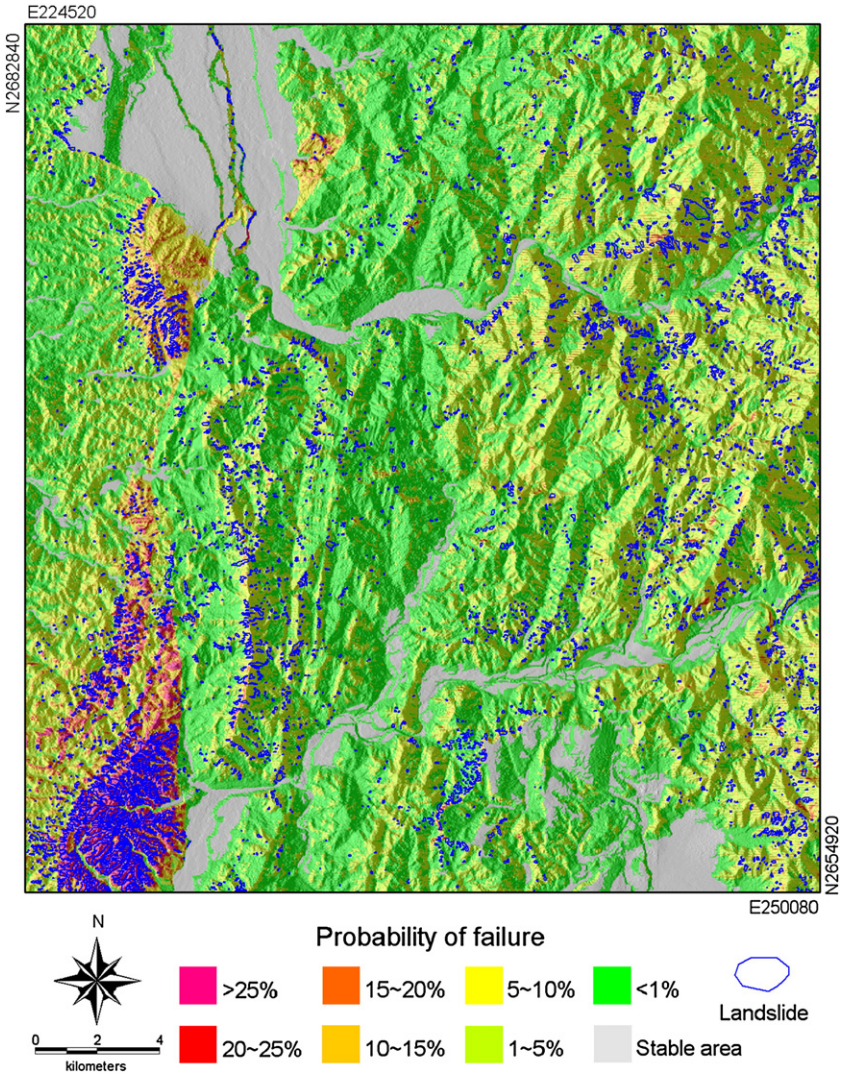

Fig. 9. Landslide susceptibility map of the Kuohsing quadrangle developed using a susceptibility model trained with the Chi-Chi landslide inventory and the earthquake shaking intensity in that quadrangle. Landslides triggered by the Chi-Chi earthquake are shown.

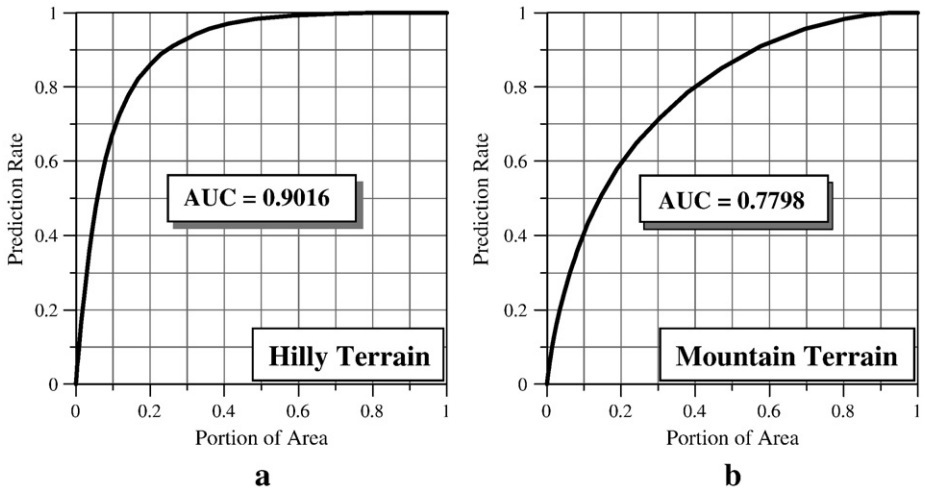

Fig. 10. Success rate curves for the Chi-Chi earthquake event in the Kuohsing quadrangle: (a) hilly terrain; (b) mountainous terrain.

shown in Fig. 10. The area under the curve (AUC) is between 0 and 1; a higher value indicates a higher prediction rate, whereas a value near 0.5 means the prediction is no better than a random guess (Chung and Fabbri, 2003). The calculated AUCs are shown in Fig. 10. The results for hilly terrain were good (AUC = 0.9016), while the results for the mountainous terrain were fairly good (AUC = 0.7798).

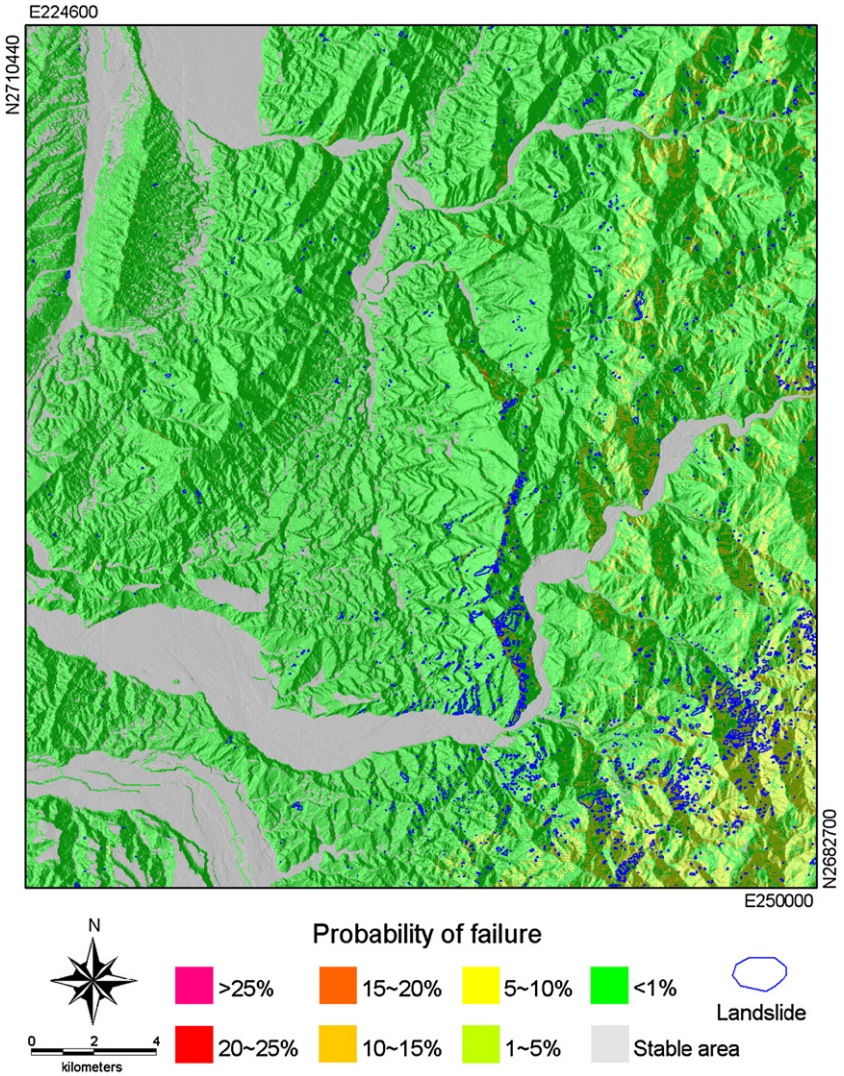

Fig. 11. Application of the Kuohsing susceptibility model to the Tungshih quadrangle. Landslides triggered by the Chi-Chi earthquake are shown.

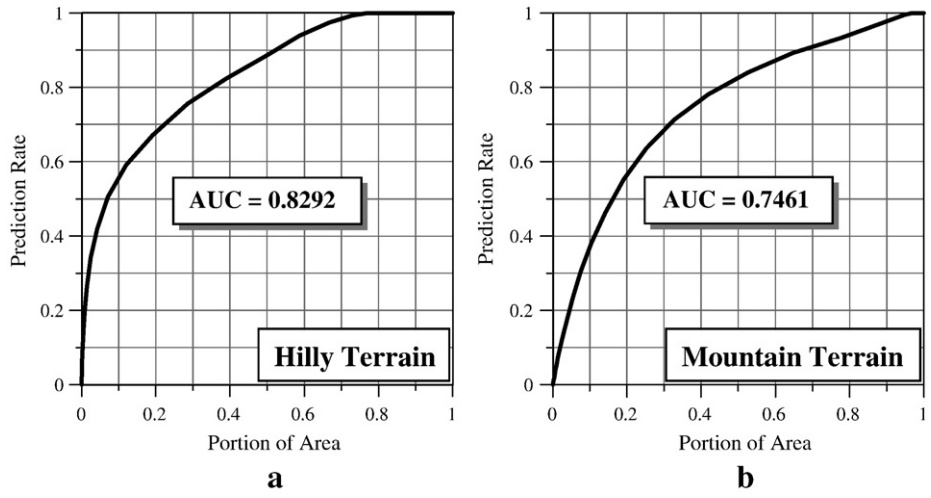

Fig. 12. Prediction rate curves for the Chi-Chi earthquake event in the Tungshih quadrangle: (a) hilly terrain; (b) mountainous terrain.

4.2. Validation in the Tungshih quadrangle

The same data sources and processing procedure were used to validate the susceptibility model for the Tungshih quadrangle. Rating curve and factor weights obtained as a result of training in the Kuohsing quadrangle were used to calculate the LSI for each grid point at the Tungshih site. The LSIs were then transformed to indicate probability of failure using equations shown in Fig. 8. The map of the susceptibility classes for the grid points in this quadrangle is shown in Fig. 11.

We also constructed an event-based landslide inventory for the Tungshih quadrangle to validate the susceptibility model. A comparison of the susceptibility map and event-triggered landslides (Fig. 11) shows a similar pattern of correspondence between landslides and high susceptibility. We calculated prediction rate curve (Chung and Fabbri, 1999) using the Tungshih landslide data which are plotted in Fig. 12. The prediction rate for the Tungshih quadrangle was less than that at the Kuohsing quadrangle. The lower prediction rate was inferred to be a result of the extensive geological formation present in the Kuohsing quadrangle — the Houyenshan conglomerate, where numerous landslides were triggered by the Chi-Chi earthquake, not being present in the Tungshih quadrangle.

5. Discussions

Is this statistical approach to earthquake-induced landslide susceptibility feasible, efficient and reliable? We will now discuss in detail some important points regarding EB-LSA as well as future prospects for the new approach and problems it may encounter. The advantages and disadvantages of this new method will also be discussed.

5.1. The methodology

The present EB-LSA differs from traditional statistical LSAs in two ways. First, instead of a multi-temporal landslide inventory, an event-based landslide inventory is used, and second, the triggering factor is emphasized. There is a very important correlation between the usage of an event-based landslide inventory and the usage of a triggering factor. Without the event-based landslide inventory, a triggering factor is not significant; without the triggering factor, a single-period landslide inventory is not temporally meaningful.

Discriminant analysis was adopted in the statistical method used in this study to find the best linear function, giving the greatest separation between the landslide group and the non-landslide group, which makes it easier to divide the region into successive classes representing different grades of slope stability. In this case, the normality of the factor is not as important for the discriminant function, because it is not seriously affected by limited departures from normality (Davis, 2002) (If it is used for classification purposes, then normality is important). However, category-type data is still not valid in a discriminant analysis. Here, category-type data — lithology was rated according to the landslide ratio, meaning that each lithologic unit was given a numerical value. The normality of the lithology factor, as expected, is not good. This factor should not be used in discriminant analysis where classification is the purpose.

If all factors are independent, the coefficients of the discriminant function can be used as the factor weights. However, inter-factor dependencies are common, as can be seen from the correlation coefficients in Table 4. The correlation coefficients between the factors used in this study ranged from − 0.11 to 0.53. To some extent, the coefficients of the discriminant function do not fully represent the weightings, so they must be used with caution. The triggering factor — AI also has some dependency on other factors, although the correlation coefficients are relatively small. It can thus be used as an independent factor to some extent defined in a later section.

The landslide inventory is used only for training the statistical model during EB-LSA, so some small landslides are missed is not important. In other words, not all of the landslide data are needed to establish a susceptibility model. This has been confirmed by Weirich and Blesius (2007). The key is to establish an event-based landslide inventory reflecting the triggering event. The use of high temporal resolution remotely sensed images is very important in order to find the landslides actually triggered by the event of interest.

5.2. Triggering factor

The triggering factor is important in a single-period landslide susceptibility study. In our case, it is the AI. The groundwater was

Table 4
Correlation coefficients between each two factors for both terrains in the Kuohsing quadrangle

	Litho	Slope	Slope Asp	Terra Rou	Slope Rou	Total curve	Arias Inten
Litho	1.000	0.216	−0.065	0.212	0.172	0.215	0.224
Slope	0.216	1.000	−0.110	0.528	0.436	0.259	0.249
Slope Asp	−0.065	−0.110	1.000	−0.020	−0.090	−0.099	−0.088
Terra Rou	0.212	0.528	−0.020	1.000	0.456	0.467	0.068
Slope Rou	0.172	0.436	−0.090	0.456	1.000	0.473	0.146
Total Curve	0.215	0.259	−0.099	0.467	0.473	1.000	0.175
Arias Inten	0.224	0.249	−0.088	0.068	0.146	0.175	1.000

Note: Abbreviations are all the same as those in Table 3.

evaluated as less important in the analysis, for the Chi-Chi earthquake occurred on dry season (it was all fine days in central western Taiwan during 5days before and 3months after the earthquake) and the shallow slides involved only loose colluvium.

One problem with earthquake intensity data is that strong-motion stations are not usually widely distributed in areas where landslides are most likely to occur. The interpolation of intensity values from the few stations available to grid points in mountainous areas is difficult and usually not effective. In this study, we adopted an empirical formula from Lin and Lee (2003) to solve the topographic amplification problem, to improve the interpolation of the Arias intensity in the study area, which did result in a better LSA model. However, the empirical formula is only good for a first-order approximation, since the topographic amplification in not simply proportional to the local height relative to riverbed. Topographic amplification can also be affected by such factors as lithology, geologic structure, and ridge sharpness (Celebi, 1987; Jibson, 1987; Geli et al., 1988; Ashford et al., 1997; Murphy, 2006). Simulations and the application of multivariate geostatistical methods may be needed to improve future results.

5.3. Causative factors

Causative factors are the basis of an LSA; as many as 40 factors have been used in the building of discriminant LSA models (Guzzetti et al., 1999). However, to make the LSA model more compact and effective, we must consider the availability, effectiveness, and independence of each factor. In this study, we found only 6 causative factors that met these requirements and were used to build our susceptibility model. One of these, the terrain roughness factor, was removed after the first run, because it was so highly dependent on the slope factor (the correlation coefficient is as high as 0.95). It was added back to the analysis only after being processed with a high-pass filter to remove regional undulations, while preserving local character of the roughness. (After this treatment, the correlation coefficient between terrain roughness and slope was reduced to 0.53).

Some factors, such as distance from the fault, though deemed important in the beginning, were found to be ineffective after standardized difference testing, and so were screened out during factor selection. Different sorts of curvature (i.e., plan curvature, profile curvature, and tangential curvature, Wilson and Gallant, 2000) were also tested during the selection process. Ohlmacher (2007) suggested that hillsides with planar plan curvature have the highest probability for landslides in regions dominated by earth flows and earth slides in clayey soils. In our case, however, the slopes were covered by loose colluvium soil. Our test found the total curvature to be the most effective factor for curvature, so this was used in the analysis.

The afore-mentioned selection process and the entire EB-LSA have already been applied to the Kuohsing, Taipei (northern Taiwan), Yinlin (southern Taiwan), and Yuli (eastern Taiwan) test sites in the CGS project, for which there was common agreement on the selection features (Lee et al., 2005). Further study should confirm whether these findings fit local site conditions, so that an optimum selection may be made.

Many causative factors, such as the slope gradient, slope aspect, terrain roughness, and curvature have been derived from a DEM. The resolution and accuracy have a direct influence on the quality of these factors. The 40 m × 40 m DEM used in this study was developed from aerial photogrammetry for rectification of 1/5000 scale photo-based contour maps. The accuracy was judged sufficient to produce 1/50,000 scale landslide susceptibility maps for the CGS project. Finer resolution and more accurate DEM could be prepared from LIDAR data to further improve the landslide susceptibility model in future.

The geologic data, which included lithology, fault location, were derived from the 1/50,000 scale geologic maps produced by the CGS. This, too, was accurate enough to produce 1/50,000 scale landslide susceptibility maps. However, it was found that adjustment of the extent of alluvium and river terraces (based on the 1 to 5000 scale photo-based maps in GIS) is needed to improve the quality.

Other factors, such as the total slope height, topographic index (Kirkby, 1975), distance from a road, distance from a fault, distance from a river head, distance from a river bend, and NDVI, were found to be less effective in the interpretation of shallow earthquake-induced landslides. The height relative to riverbed was included during processing of the triggering factors but not in the analysis. Some of these factors, however, have been found to be important for storm-induced landslide analysis. This will be discussed in a separate paper currently in preparation.

5.4. Comparison with deterministic methods

Both LSA and deterministic methods (e.g. Jibson and Keefer, 1993) have advantages and disadvantages. A deterministic method requires the calculation of the limit-equilibrium slope stability, the needs of the strength parameters, failure-surface depth and pore-water pressures for every point in the study area. This causes serious problems in terms of the acquisition and control of spatial variability of the input parameters (Hutchinson, 1995; Guzzetti et al., 1999). Indirect determination of input parameters by back-analysis and/or other methods may help, but the results may not be as good as those obtained with a multivariate method (Lee, 2006). This uncertainty remains difficult to evaluate. The spatial variability of these parameters is also not controlled (Guzzetti et al., 1999). By contrast, with the statistical method, one does not need the strength parameters, failure depth, or pore-water pressure data for the analysis. The EB-LSA is therefore a more reliable method for producing a landslide susceptibility map than a deterministic method.

A disadvantage of EB-LSA is that the physical meaning of some susceptibility factors may be unclear. This defect need to be further studied so that each factor also has a clear physical meaning. The EB-LSA is to some extent physically-based. For example, instead of the slope angle, we used the slope gradient, which is approximately inversely proportional to the factor of safety in an analytical slope-stability model. Moreover, instead of the PGA, we used the AI (which integrates the entire record of earthquake shaking) as the intensity measure for triggering the landslide. An additional topographic amplification factor for the Arias intensity was also used.

Once the parameters required by the model are available, the deterministic earthquake-induced landslide model can be used anywhere. However, an LSA (or EB-LSA) model may be applicable only to the small region where the model was trained. The use of an LSA or EB-LSA over a wider region requires special consideration. In the CGS landslide project, the whole of Taiwan was divided into several terrain zones, with an LSA model trained for each specific type of terrain (Lee et al., 2005).

5.5. Landslide prediction during a scenario

Both the deterministic method and the EB-LSA are capable of landslide prediction during a scenario event, provided the earthquake intensity and the Newmark displacement (for the deterministic method) or the susceptibility index (for the EB-LSA) is known for each study point. A curve representing landslide ratio versus Newmark displacement can be used in a deterministic earthquake-induced landslide study to indicate the spatial probability of a landslide at any point where the Newmark displacement is known (Jibson et al., 2000). Similarly, in the EB-LSA, the curve representing the landslide ratio versus the LSI (e.g. Fig. 9) can be used to indicate the spatial probability of landslide occurrence during an earthquake event at any point where the LSI is known.

The temporal probability of shaking intensity during an earthquake event may be obtained via a probabilistic seismic hazard analysis of the AI (Jibson, 1993; Jibson et al., 2000; Romeo, 2000). By

combining spatial probability and temporal probability, we may establish a probabilistic landslide hazard model. Examples show that this type of model can help to reveal hazard probability in Taiwan (Liao, 2004; Lee et al., 2005).

In other LSAs, temporal information most commonly comes from the multi-temporal landslide inventory and the probability is determined thereafter (Guzzetti et al., 1999, 2005). Zêzere et al. (2004) utilized a multi-temporal landslide inventory and Bayesian statistics to build a susceptibility model. They further used storm-event data to determine the conditional probability that a pixel would be affected by a shallow translational slide during a scenario event. The conditional probability was calculated based on the event-induced landslide areas and the prediction areas in a susceptibility class. Triggering factors were not actually used in the building of the model, or in the prediction.

When using the EB-LSA model for prediction, the value of a triggering factor can not over exceed the value used during establishment of the model. In other words, the range of values for a triggering factor to be used for prediction must be similar to the range used in the training of the model. Also, the inherence of past condition (like land-use and soil moisture) must be preserved so that the causative factors used in establishing the model may represent the background condition in prediction. Since the Chi-Chi earthquake occurred during a dry season, therefore the susceptibility model established using the Chi-Chi data set is valid for application also in a dry season. In Taiwan and in this study area, hill slopes are commonly covered by loose colluvium. Soil moisture is low in fine days and land-use does not affect the soil moisture very much. Unless in the case of a storm, the causative factors may preserve the inherence of past condition to some extents and the susceptibility model may still be used for prediction. Extreme condition of earthquake during a storm is not valid for the present model, but it is uncommon.

6. Conclusions and recommendations

We proposed a method for the event-based landslide susceptibility analysis (EB-LSA) of shallow earthquake-induced landslides. We used a multivariate statistical approach with discriminant analysis. Results of the analysis were good, provided that careful validation at a neighboring region was made. We conclude that the present methodology and working procedure are feasible, and that the susceptibility model has the potential to predict landslides after an earthquake, provided the range of shaking intensity is similar to that used in building the model.

The Arias intensity is used as the triggering factor in the susceptibility analysis, and this factor makes the susceptibility model temporally significant. It is also found to be the most effective factor for interpreting landslide distribution and thus improves the quality of the model.

EB-LSA has an advantage over deterministic methods in that it does not require failure depth, material strength, or groundwater data, and may have a better prediction rate. However, a deterministic model can be used anywhere once the parameters required by the model are available. An LSA model, by contrast, may be applicable only to the small region where the model was trained, unless special considerations, like those used for the CGS landslide project discussed above, are taken.

Since the deterministic method is fully physically-based, it is recommended that it be used if data on potential failure depth, material strength, and groundwater parameters are available for the study region. If not, the EB-LSA, is to some extent physically-based, is suggested. More physically-based treatment of the susceptibility factors should be considered in the future to improve the susceptibility model.

Acknowledgements

This research was supported by the Central Geological Survey (CGS), Ministry of Economic Affairs, Taiwan, under the Landslide Research Project. The authors are deeply appreciative to Director C.C. Lin of the CGS for his concern for this project and for his helpful hints. The authors would also like to express their appreciation to the several reviewers of this project for their enthusiastic advice and valuable suggestions. Special thanks are due to Dr. D.K. Keefer of the U.S. Geological Survey, Menlo Park, for his helpful discussion and critical reading of this manuscript. Dr. Roberto Romeo, an anonymous reviewer and Editor Giovanni Crosta provided constructive comments.

References

Arias, A., 1970. A measure of earthquake intensity. In: Hansen, R.J. (Ed.), Seismic Design for Nuclear Power Plants. MIT Press, Cambridge, Massachusetts, pp. 438–483.
Ashford, S.A., Sitar, N., Lysmer, J., Deng, N., 1997. Topographic effects on the seismic response of steep slopes. Bulletin of the Seismological Society of America 87 (3), 701–709.
Bonilla, M.G., 1975. A review of recently active fault in Taiwan. U.S. Geological Survey Open-File Report 75–41 58 pp.
Bonilla, M.G., 1977. Summary of Quaternary faulting and elevation changes in Taiwan. Memoir of the Geological Society of China 2, 43–55.
Bowin, C., Lu, R.S., Lee, C.S., Schouten, H., 1978. Plate convergence and accretion in the Taiwan–Luzon region. American Association of Petroleum Geologists Bulletin 62, 1645–1972.
Carrara, A., 1983. Multivariate models for landslide hazard evaluation. Mathematical Geology 15 (3), 403–427.
Carrara, A., Cardinali, M., Guzzetti, F., Reichenbach, P., 1995. GIS technology in mapping landslide hazard. In: Carrara, A., Guzzetti, F. (Eds.), Geographical Information Systems in Assessing Natural Hazards. Kluwer Academic Publishers, Dordrecht, The Netherlands, pp. 135–175.
Celebi, M., 1987. Topographical and geological amplifications determined from strong-motion and aftershock records of the 3 march 1985 Chile earthquake. Bulletin of the Seismological Society of America 77 (4), 1147–1167.
Chai, B.H.T., 1972. Structure and tectonic evolution of Taiwan. American Journal of Science 272, 389–422.
Chung, C.F., 2006. Using likelihood ratio functions for modeling the conditional probability of occurrence of future landslides for risk assessment. Computer and Geosciences 32, 1052–1068.
Chung, C.F., Fabbri, A.G., 1999. Probabilistic prediction models for landslide hazard mapping. Photogrammetric Engineering and Remote Sensing 65 (12), 1389–1399.
Chung, C.F., Fabbri, A.G., 2003. Validation of spatial prediction models for landslide hazard mapping. Natural Hazards 30, 451–472.
Dadson, S.J., Hovious, N., Chen, H., Dade, B.W., Willett, S.D., Hu, J.C., Horng, M.J., Chen, M.C., Stark, C.P., Lague, D., Lin, J.C., 2003. Links between erosion, runoff variability, and seismicity in the Taiwan orogen. Nature 426, 648–651.
Darragh, B., Silva, W., Gregor, N., 2004. Strong motion record processing for the PEER center. Proceedings of COSMOS Invited Workshop on Strong-Motion Record Processing, Richmond, Calif, USA, pp. 26–27.
Davis, J.C., 2002. Statistics and data analysis in geology, 3rd ed. John Wiley and Sons. 638 pp.
ERDAS, 1997. ERDAS Field Guide, 5th Edition. ERDAS, Inc., Atlanta, Georgia, USA. 672 pp.
Geli, L., Bard, P.-Y., Jullien, B., 1988. The effect of topography on earthquake ground motion: a review and new results. Bulletin of the Seismological Society of America 78 (1), 42–63.
Goovaerts, P., 1997. Geostatistics for natural resources evaluation. Oxford University Press, Oxford. 483 pp.
Guzzetti, F., Carrara, A., Cardinali, M., Reichenbach, P., 1999. Landslide hazard evaluation: a review of current techniques and their application in a multi-scale study, Central Italy. Geomorphology 31, 181–216.
Guzzetti, F., Reichenbach, P., Cardinali, M., Galli, M., Ardizzone, F., 2005. Probabilistic landslide hazard assessment at the basin scale. Geomorphology 72, 272–299.
Harp, E.L., Wilson, R.C., 1995. Shaking intensity thresholds for rock falls and slides: evidence from 1987 Whittier Narrows and Superstition Hills earthquake strong-motion records. Bulletin of the Seismological Society of America 85 (6), 1739–1757.
Ho, C.S., 1975. An introduction to the geology of Taiwan, explanatory text of the geologic map of Taiwan. Ministry of Economic Affairs, Republic of China. 312 pp.
Hsu, M.T., 1971. Seismicity of Taiwan and some related problem. Bulletin of the International Institute of Seismology and Earthquake Engineering 8, 41–160.
Hutchinson, J.N., 1995. Landslide hazard assessment. In: Bell, D.H. (Ed.), Landslides, pp. 1805–1841.
Jibson, R.W., 1987. Summary of research on the effects of topographic amplification of earthquake shaking on slope stability. U.S. Geological Survey Open-File Report 87–268 166 pp.
Jibson, R.W., 1993. Predicting earthquake-induced landslide displacements using Newmark's sliding block analysis. Transportation Research Board Record 1411, 9–17.
Jibson, R.W., Keefer, D.K., 1993. Analysis of the seismic origin of landslides: examples from the New Madrid seismic zone. Geological Society of America Bulletin 105 (4), 521–536.
Jibson, R.W., Harp, E.L., Michael, J.A., 1998. A method for producing digital probabilistic seismic landslide hazard maps: an example from the Los Angeles, California Area. U.S. Geological Survey Open-File Report 98–113 17 pp.
Jibson, R.W., Harp, E.L., Michael, J.A., 2000. A method for producing digital probabilistic seismic landslide hazard maps. Engineering Geology 58, 271–289.
Kao, H., Chen, W.P., 2000. The Chi-Chi earthquake sequence: active out-of-sequence thrust faulting in Taiwan. Science 288, 2346–2349.

Keefer, D.K., Larsen, M.C., 2007. Assessing landslide hazards. Sciences 316, 1136–1137.
Kirkby, M.J., 1975. Hydrograph modelling strategies. In: Peel, R., Chisholm, M., Haggett, P. (Eds.), Process in Physical and Human Geography. Heinemann, London, pp. 69–90.
Lee, C.T., 2006. Methodology for estimation of earthquake-induced landslide probability and result evaluation. Geophysical Research Abstract 8, 05759.
Lee, C.T., Pan, K.L., Lin, M.L., 2005. Research of landslide susceptibility analyses. Taiwan Central Geological Survey Open-File Report 94-18 474 pp.
Liao, C.W., 2004. Probabilistic Hazard Analysis of Earthquake-Induced Landslides — an Example from Kuohsing, Taiwan. Ph.D. Thesis of Institute of Geophysics, National Central University, 120p. (in Chinese with English abstract).
Liao, H.W., Lee, C.T., 2000. Landsides triggered by the Chi-Chi Earthquake. Proceedings of the 21st Asian Conference on Remote Sensing, vol. 1&2, pp. 383–388.
Lin, P.S., Lee, C.T., 2003. Arias intensity in landslide susceptibility analysis. Proceeding of 2003 Annual Meeting of Chinese geophysical Society (Taiwan), pp. 91–96 (in Chinese with English abstract).
Lin, Y.H., 2003. Application of neural networks to landslide susceptibility analysis. M.S. Thesis of Institute of Applied Geology, National Central University, 81p. (in Chinese with English abstract).
Liu, J.G., 2000. Smoothing filter-based intensity modulation: a spectral preserve image fusion technique for improving spatial details. International Journal of Remote Sensing 21 (18), 3461–3472.
Ma, K.F., Lee, C.T., Tsai, Y.B., 1999. The Chi-Chi, Taiwan earthquake: large surface displacements on an inland fault. EOS Transactions, American Geophysical Union 80 (50), 605–611.
Murphy, W., 2006. The role of topographic amplification on the initiation of rock slopes failures during earthquakes. In: Evans, et al. (Ed.), Landslides from Massive Rock Slope Failure, pp. 139–154.
Ohlmacher, G.C., 2007. Plan curvature and landslide probability in regions dominated by earth flows and earth slides. Engineering Geology 91, 117–134.
Pan, K.L., Lee, C.T., Wei, C.Y., Lee, J.F., Liao, C.W., Chang, C.W., Lin, Y.H., Lin, S.Y., 2004. Inventory of event-induced landslides by using space imagery. Proceeding of International Symposium on Landslide and Debris Flow Hazard Assessment, pp. 1–1–1-11.
Paruelo, J.M., Garbulsky, M.F., Guerschman, J.P., Jobbagy, E.G., 2004. Two decades of Normalized Difference Vegetation Index changes in South America: identifying the imprint of global change. International Journal of Remote Sensing 25 (14), 2793–2806.
Romeo, R., 2000. Seismically induced landslide displacements: a predictive model. Engineering Geology 58 (3–4), 337–351.
Teng, L.S., 1990. Geotectonic evolution of late Cenozoic arc–continent collision in Taiwan. Tectonophysics 183, 57–76.
Tsai, Y.B., Teng, T.L., Chiu, J.M., Liu, H.L., 1977. Tectonic implications of the seismicity in the Taiwan region. Memoir of the Geological Society of China 2, 13–41.
van Western, C.J., van Asch, T.W.J., Soeters, R., 2006. Landslide hazard and risk zonation — why is it still so difficult? Bulletin of Engineering Geology and Environment 65, 167–184.
Varnes, D.J., 1984. Landslide hazard zonation: a review of principles and practice. UNESCO Press, Praris. 63 pp.
Weirich, F., Blesius, L., 2007. Comparison of satellite and air photo based landslide susceptibility maps. Geomorphology 87, 352–364.
Wilson, J.P., Gallant, J.C., 2000. Terrain analysis. John Wiley & Sons, Inc.. 479 pp.
Wilson, R.C., Keefer, D.K., 1985. Predicting areal limits of earthquake-induced landsliding. U.S. Geological Survey Professional Paper 1360, 317–345.
Wu, F.T., 1978. Recent tectonics of Taiwan. Journal of Physics of the Earth 26, 265–299 (Suppl.).
Yu, S.B., Chen, H.Y., Kou, L.C., 1997. Velocity field of GPS stations in the Taiwan area. Tectonophysics 274, 41–59.
Zêzere, J.L., Reis, E., Garcia, R., Oliveira, S., Rodrigues, M.L., Vieira, G., Ferreira, A.B., 2004. Integration of spatial and temporal data for the definition of different landslide hazard scenarios in the area north of Lisbon (Portugal). Natural Hazards and Earth System Sciences 4, 133–146.